# Updated measurements of absolute $D^+$ and $D^0$ hadronic branching fractions and $\sigma(e^+e^- \to D\bar{D})$ at $E_{\rm cm} = 3774$ MeV

G. Bonvicini,[1] D. Cinabro,[1] M. J. Smith,[1] P. Zhou,[1] P. Naik,[2] J. Rademacker,[2] K. W. Edwards,[3] R. A. Briere,[4] H. Vogel,[4] J. L. Rosner,[5] J. P. Alexander,[6] D. G. Cassel,[6] R. Ehrlich,[6] L. Gibbons,[6] S. W. Gray,[6] D. L. Hartill,[6] B. K. Heltsley,[6] D. L. Kreinick,[6] V. E. Kuznetsov,[6] J. R. Patterson,[6] D. Peterson,[6] D. Riley,[6] A. Ryd,[6] A. J. Sadoff,[6] X. Shi,[6,*] W. M. Sun,[6] S. Das,[7] J. Yelton,[7] P. Rubin,[8] N. Lowrey,[9] S. Mehrabyan,[9] M. Selen,[9] J. Wiss,[9] J. Libby,[10] M. Kornicer,[11] R. E. Mitchell,[11] D. Besson,[12] T. K. Pedlar,[13] D. Cronin-Hennessy,[14] J. Hietala,[14] S. Dobbs,[15] Z. Metreveli,[15] K. K. Seth,[15] A. Tomaradze,[15] T. Xiao,[15] A. Powell,[16] C. Thomas,[16] G. Wilkinson,[16] D. M. Asner,[17] G. Tatishvili,[17] J. Y. Ge,[18] D. H. Miller,[18] I. P. J. Shipsey,[18,†] B. Xin,[18] G. S. Adams,[19] J. Napolitano,[19] K. M. Ecklund,[20] J. Insler,[21] H. Muramatsu,[21] L. J. Pearson,[21] E. H. Thorndike,[21] M. Artuso,[22] S. Blusk,[22] R. Mountain,[22] T. Skwarnicki,[22] S. Stone,[22] J. C. Wang,[22] L. M. Zhang,[22] P. U. E. Onyisi[23]

(CLEO Collaboration)

[1]*Wayne State University, Detroit, Michigan 48202, USA*
[2]*University of Bristol, Bristol BS8 1TL, United Kingdom*
[3]*Carleton University, Ottawa, Ontario K1S 5B6, Canada*
[4]*Carnegie Mellon University, Pittsburgh, Pennsylvania 15213, USA*
[5]*University of Chicago, Chicago, Illinois 60637, USA*
[6]*Cornell University, Ithaca, New York 14853, USA*
[7]*University of Florida, Gainesville, Florida 32611, USA*
[8]*George Mason University, Fairfax, Virginia 22030, USA*
[9]*University of Illinois, Urbana-Champaign, Illinois 61801, USA*
[10]*Indian Institute of Technology Madras, Chennai, Tamil Nadu 600036, India*
[11]*Indiana University, Bloomington, Indiana 47405, USA*
[12]*University of Kansas, Lawrence, Kansas 66045, USA*
[13]*Luther College, Decorah, Iowa 52101, USA*
[14]*University of Minnesota, Minneapolis, Minnesota 55455, USA*
[15]*Northwestern University, Evanston, Illinois 60208, USA*
[16]*University of Oxford, Oxford OX1 3RH, United Kingdom*
[17]*Pacific Northwest National Laboratory, Richland, Washington 99352, USA*
[18]*Purdue University, West Lafayette, Indiana 47907, USA*
[19]*Rensselaer Polytechnic Institute, Troy, New York 12180, USA*
[20]*Rice University, Houston, Texas 77005, USA*
[21]*University of Rochester, Rochester, New York 14627, USA*
[22]*Syracuse University, Syracuse, New York 13244, USA*
[23]*University of Texas at Austin, Austin, Texas 78712, USA*

(Received 24 December 2013; published 2 April 2014)

Utilizing the full CLEO-c data sample of 818 pb$^{-1}$ of $e^+e^-$ data taken at the $\psi(3770)$ resonance, we update our measurements of absolute hadronic branching fractions of charged and neutral $D$ mesons. We previously reported results from subsets of these data. Using a double tag technique we obtain branching fractions for three $D^0$ and six $D^+$ modes, including the reference branching fractions $\mathcal{B}(D^0 \to K^-\pi^+) = (3.934 \pm 0.021 \pm 0.061)\%$ and $\mathcal{B}(D^+ \to K^-\pi^+\pi^+) = (9.224 \pm 0.059 \pm 0.157)\%$. The uncertainties are statistical and systematic, respectively. In these measurements we include the effects of final-state radiation by allowing for additional unobserved photons in the final state, and the systematic errors include our estimates of the uncertainties of these effects. Furthermore, using an independent measurement of the luminosity, we obtain the cross sections $\sigma(e^+e^- \to D^0\bar{D}^0) = (3.607 \pm 0.017 \pm 0.056)$ nb and $\sigma(e^+e^- \to D^+D^-) = (2.882 \pm 0.018 \pm 0.042)$ nb at a center of mass energy, $E_{\rm cm} = 3774 \pm 1$ MeV.

DOI: 10.1103/PhysRevD.89.072002 PACS numbers: 13.25.Ft

## I. INTRODUCTION

Precision measurements of absolute hadronic $D$ meson branching fractions are essential for both charm and beauty physics. For example, determination of the

[*]Present address: Purdue University, West Lafayette, Indiana 47907, USA.
[†]Present address: University of Oxford, Oxford OX1 3RH, United Kingdom.

 

Cabibbo-Kobayashi-Maskawa (CKM) [1,2] matrix element $|V_{cb}|$ utilizing the exclusive decay $B \to D^* \ell \nu$ with full $D^*$ reconstruction requires knowledge of the absolute $D$ meson branching fractions [3]. We report absolute measurements of three $D^0$ and six $D^+$ branching fractions (averaged between $D^0$ and $\bar{D}^0$ or $D^+$ and $D^-$) for the Cabibbo-favored decays $D^0 \to K^-\pi^+$, $D^0 \to K^-\pi^+\pi^0$, $D^0 \to K^-\pi^+\pi^+\pi^-$, $D^+ \to K^-\pi^+\pi^+$, $D^+ \to K^-\pi^+\pi^+\pi^0$, $D^+ \to K^0_S\pi^+$, $D^+ \to K^0_S\pi^+\pi^0$, $D^+ \to K^0_S\pi^+\pi^+\pi^-$, and the Cabibbo-suppressed decay $D^+ \to K^+K^-\pi^+$. We call $\mathcal{B}(D^0 \to K^-\pi^+)$ and $\mathcal{B}(D^+ \to K^-\pi^+\pi^+)$ reference branching fractions because most $D^0$ and $D^+$ branching fractions are determined from ratios to one of these branching fractions [3].

The data sample was produced in $e^+e^-$ collisions at the Cornell Electron Storage Ring (CESR) and collected with the CLEO-c detector [4–7]. It consists of 818 pb$^{-1}$ of integrated luminosity collected on the $\psi(3770)$ resonance, at a center-of-mass energy $E_{\rm cm} = 3774 \pm 1$ MeV. We previously reported results based on 56 pb$^{-1}$ [8] and 281 pb$^{-1}$ [9] subsamples of these data. These final measurements from CLEO supersede the earlier CLEO results. Because the principal analysis technique is unchanged and was documented in great detail in Ref. [9], we will briefly review the procedure here and focus primarily on significant improvements.

In accordance with our previous measurements [8,9], we employ a "double tagging" technique pioneered by the MARK III Collaboration [10,11] to measure these branching fractions. This technique takes advantage of a unique feature of data taken at a center-of-mass energy near the peak of the $\psi(3770)$ resonance in $e^+e^-$ collisions. This resonance is just above the threshold for $D\bar{D}$ production, so only $D^0\bar{D}^0$ and $D^+D^-$ pairs are produced without additional hadrons in the final states. We select "single tag" (ST) events in which either a $D$ or $\bar{D}$ is reconstructed without reference to the other particle and "double tag" (DT) events in which both the $D$ and $\bar{D}$ are reconstructed. Then we determine absolute branching fractions for $D^0$ or $D^+$ decays from the fraction of DT events in our ST samples.

Letting $N_{D\bar{D}}$ be the number of $D\bar{D}$ events (either $D^0\bar{D}^0$ or $D^+D^-$) produced in the experiment, the observed yields, $y_i$ and $y_{\bar{\jmath}}$, of reconstructed $D \to i$ and $\bar{D} \to \bar{\jmath}$ ST events will be

$$y_i = N_{D\bar{D}}\mathcal{B}_i\epsilon_i \quad \text{and} \quad y_{\bar{\jmath}} = N_{D\bar{D}}\mathcal{B}_j\epsilon_{\bar{\jmath}}, \tag{1}$$

where $\mathcal{B}_i$ and $\mathcal{B}_j$ are branching fractions for $D \to i$ and $D \to j$, with the assumption that charge-conjugation parity ($CP$) violation is negligible so that $\mathcal{B}_j = \mathcal{B}_{\bar{\jmath}}$. However, the efficiencies $\epsilon_j$ and $\epsilon_{\bar{\jmath}}$ for detection of these modes may not be the same due to the charge dependencies of cross sections for the scattering of pions and kaons on the nuclei of the detector material. Furthermore, the DT yield for $D \to i$ (signal mode) and $\bar{D} \to \bar{\jmath}$ (tagging mode) will be

$$y_{i\bar{\jmath}} = N_{D\bar{D}}\mathcal{B}_i\mathcal{B}_j\epsilon_{i\bar{\jmath}}, \tag{2}$$

where $\epsilon_{i\bar{\jmath}}$ is the efficiency for detecting double tag events in modes $i$ and $\bar{\jmath}$. A combination of Eqs. (1) and (2) yields an absolute measurement of the branching fraction $\mathcal{B}_i$,

$$\mathcal{B}_i = \frac{y_{i\bar{\jmath}}}{y_{\bar{\jmath}}}\frac{\epsilon_{\bar{\jmath}}}{\epsilon_{i\bar{\jmath}}}. \tag{3}$$

Note that $\epsilon_{i\bar{\jmath}} \approx \epsilon_i\epsilon_{\bar{\jmath}}$, so $\epsilon_{i\bar{\jmath}}/\epsilon_{\bar{\jmath}} \approx \epsilon_i$, and the measured value of $\mathcal{B}_i$ is quite insensitive to the value of $\epsilon_{\bar{\jmath}}$.

We utilize a least-squares technique to extract branching fractions and $N_{D\bar{D}}$ by combining ST and DT yields. Although the $D^0$ and $D^+$ yields are statistically independent, systematic effects and misreconstruction resulting in cross feeds among the decay modes introduce correlations among their uncertainties. Therefore, we fit $D^0$ and $D^+$ parameters simultaneously by minimizing a $\chi^2$ that includes statistical and systematic uncertainties and their correlations for all experimental inputs [12]. In the fit, we include the ST and DT efficiencies and—as described below—correct the ST and DT yields for backgrounds that peak in the regions of the signal peaks.

## II. DETECTOR AND RECONSTRUCTION

We reconstruct charged tracks in the CLEO-c detector using the 47-layer drift chamber [5] and the coaxial 6-layer vertex drift chamber [7]. For tracks that traverse all layers of the drift chamber, the root-mean-square (rms) momentum resolution is approximately 0.6% at $p = 1$ GeV/$c$. We detect photons in an electromagnetic calorimeter containing about 7800 CsI(Tl) crystals [4], whose rms photon energy resolution is 2.2% at $E_\gamma = 1$ GeV, and 5% at $E_\gamma = 100$ MeV. The solid angle for detection of charged tracks and photons is 93% of $4\pi$. Particle identification (PID) information to separate $K^\pm$ from $\pi^\pm$ is provided by measurements of ionization ($dE/dx$) in the central drift chamber [5] and by a cylindrical ring-imaging Cherenkov (RICH) detector [6]. Below about $p = 0.7$ GeV/$c$, separation using only $dE/dx$ is very effective and we utilize this technique alone. Above that momentum, we combine information from $dE/dx$ and the RICH detector when both are available. The solid angle of the RICH detector is about 86% of the solid angle of the tracking system, leading to a modest decrease in PID effectiveness above $p = 0.7$ GeV/$c$. We describe the PID techniques and performance in more detail in Ref. [9]. We reconstruct $K^0_S$ in the decay mode $K^0_S \to \pi^+\pi^-$, without requiring PID for the charged pions.

We study the response of the CLEO-c detector utilizing a GEANT-based [13] Monte Carlo (MC) simulation of particle detection. We use EVTGEN [14] to generate $D$ and $\bar{D}$ daughters and PHOTOS [15] to simulate final-state radiation (FSR).

We identify $D$ meson candidates by their beam-constrained masses ($M_{\rm BC}$) and total energies. For each candidate, we calculate $M_{\rm BC}$ by substituting the beam energy, $E_0$, for the measured $D$ candidate energy, i.e.,

TABLE I. Single tag efficiencies, yields from data, and peaking background estimates for $D\bar{D}$ events. The efficiencies include the branching fractions for $\pi^0 \to \gamma\gamma$ and $K^0_S \to \pi^+\pi^-$ decays. Peaking backgrounds are not included in the background shape functions, so the "Data yield" values include "Peaking backgrounds." The MC simulations yielded no peaking backgrounds for a few modes, indicated by three center dots in the "Peaking background" column.

| Single tag mode | Efficiency(%) | Data yield | Peaking background |
|---|---|---|---|
| $D^0 \to K^-\pi^+$ | $65.17 \pm 0.11$ | $75177 \pm 281$ | $285 \pm 13$ |
| $\bar{D}^0 \to K^+\pi^-$ | $65.88 \pm 0.11$ | $75584 \pm 282$ | $285 \pm 13$ |
| $D^0 \to K^-\pi^+\pi^0$ | $35.28 \pm 0.07$ | $144710 \pm 439$ | $296 \pm 17$ |
| $\bar{D}^0 \to K^+\pi^-\pi^0$ | $35.62 \pm 0.07$ | $145798 \pm 441$ | $296 \pm 17$ |
| $D^0 \to K^-\pi^+\pi^+\pi^-$ | $46.82 \pm 0.09$ | $114222 \pm 366$ | $2600 \pm 262$ |
| $\bar{D}^0 \to K^+\pi^-\pi^-\pi^+$ | $47.19 \pm 0.09$ | $114759 \pm 368$ | $2600 \pm 262$ |
| $D^+ \to K^-\pi^+\pi^+$ | $54.92 \pm 0.10$ | $116545 \pm 354$ | ⋯ |
| $D^- \to K^+\pi^-\pi^-$ | $55.17 \pm 0.10$ | $117831 \pm 356$ | ⋯ |
| $D^+ \to K^-\pi^+\pi^+\pi^0$ | $28.13 \pm 0.10$ | $36813 \pm 260$ | ⋯ |
| $D^- \to K^+\pi^-\pi^-\pi^0$ | $28.21 \pm 0.10$ | $37143 \pm 261$ | ⋯ |
| $D^+ \to K^0_S\pi^+$ | $45.63 \pm 0.10$ | $16844 \pm 137$ | $81 \pm 22$ |
| $D^- \to K^0_S\pi^-$ | $45.33 \pm 0.10$ | $17087 \pm 138$ | $81 \pm 22$ |
| $D^+ \to K^0_S\pi^+\pi^0$ | $23.95 \pm 0.11$ | $38329 \pm 262$ | $110 \pm 52$ |
| $D^- \to K^0_S\pi^-\pi^0$ | $24.10 \pm 0.11$ | $38626 \pm 263$ | $110 \pm 52$ |
| $D^+ \to K^0_S\pi^+\pi^+\pi^-$ | $32.29 \pm 0.14$ | $23706 \pm 224$ | $601 \pm 226$ |
| $D^- \to K^0_S\pi^-\pi^-\pi^+$ | $32.60 \pm 0.14$ | $23909 \pm 225$ | $601 \pm 226$ |
| $D^+ \to K^+K^-\pi^+$ | $44.52 \pm 0.29$ | $10115 \pm 123$ | ⋯ |
| $D^- \to K^-K^+\pi^-$ | $44.66 \pm 0.26$ | $10066 \pm 123$ | ⋯ |

$M_{\rm BC}c^2 \equiv (E_0^2 - \mathbf{p}_D^2 c^2)^{\frac{1}{2}}$, where $\mathbf{p}_D$ is the momentum of the $D$ candidate. The beam-constrained mass has a rms resolution of about 2 MeV/$c^2$, which is dominated by the beam energy spread. For the total energy selection, we define $\Delta E \equiv E_D - E_0$, where $E_D$ is the sum of the $D$ candidate daughter energies. For further analysis, we select $D$ candidates with $M_{\rm BC}$ greater than 1.83 GeV/$c^2$ and $|\Delta E|$ within mode-dependent limits that are approximately $\pm 3\sigma$ [9]. For both ST and DT modes, we accept at most one candidate per mode per event, where conjugate modes are treated as distinct. For ST candidates, we chose the candidate with the smallest $\Delta E$, while for DT candidates, we take the candidate whose average of $D$ and $\bar{D}$ $M_{\rm BC}$ values, denoted by $\widehat{M}$, is closest to the known $D$ mass.

## III. SINGLE TAG AND DOUBLE TAG YIELDS

We extract ST and DT yields from $M_{\rm BC}$ distributions in the samples described above. We perform unbinned maximum likelihood fits in one and two dimensions for ST and DT modes, respectively, to a signal shape and one or more background components. The signal shape includes the effects of beam energy smearing, initial-state radiation, the line shape of the $\psi(3770)$, and reconstruction resolution. The background in ST modes is described by an ARGUS function [16], which models combinatorial contributions. In DT modes, backgrounds can be uncorrelated, where either the $D$ or $\bar{D}$ is misreconstructed, or correlated, where all the final-state particles in the event are correctly reconstructed but are mispartitioned among the $D$ and $\bar{D}$. In fitting the two-dimensional $M_{\rm BC}(D)$ versus $M_{\rm BC}(\bar{D})$ distribution, we model the uncorrelated background by a pair of functions, where one dimension is an ARGUS function and the other is the signal shape. We model the correlated background by an ARGUS function in $\widehat{M}$ and a Gaussian in the orthogonal variable, which is $[M_{\rm BC}(\bar{D}) - M_{\rm BC}(D)]/2$. In Ref. [9] we describe in detail the fit functions that we use and the parameters that determine these functions.

Table I gives the 18 ST data yields (without efficiency correction) and the corresponding efficiencies, which are determined from simulated events. Figure 1 shows the $M_{\rm BC}$ distributions[1] for the nine decay modes with $D$ and $\bar{D}$ candidates combined. The fitted signal and background components are overlaid. We also measure 45 DT yields in data and determine the corresponding efficiencies from simulated events. Figure 2 shows projections on the $M_{\rm BC}(D)$ axis for all (a) $D^0\bar{D}^0$ and (b) $D^+D^-$ DT candidates.

Backgrounds with smooth $M_{\rm BC}$ distributions are well represented by ARGUS functions and do not contribute to the ST and DT yields, but there are backgrounds that peak

[1]We utilize square-root scales in Fig. 1 because these scales are an excellent visual compromise between linear scales (which emphasize signals) and logarithmic scales (which emphasize backgrounds). This property results from the fact all error bars that are proportional to $\sqrt{N}$ are the same size on a square-root scale. However, the error bars in these plots for small numbers of events are somewhat larger than the others because we utilize ROOFIT [17] to produce these plots and ROOFIT error bars are 68% confidence intervals.

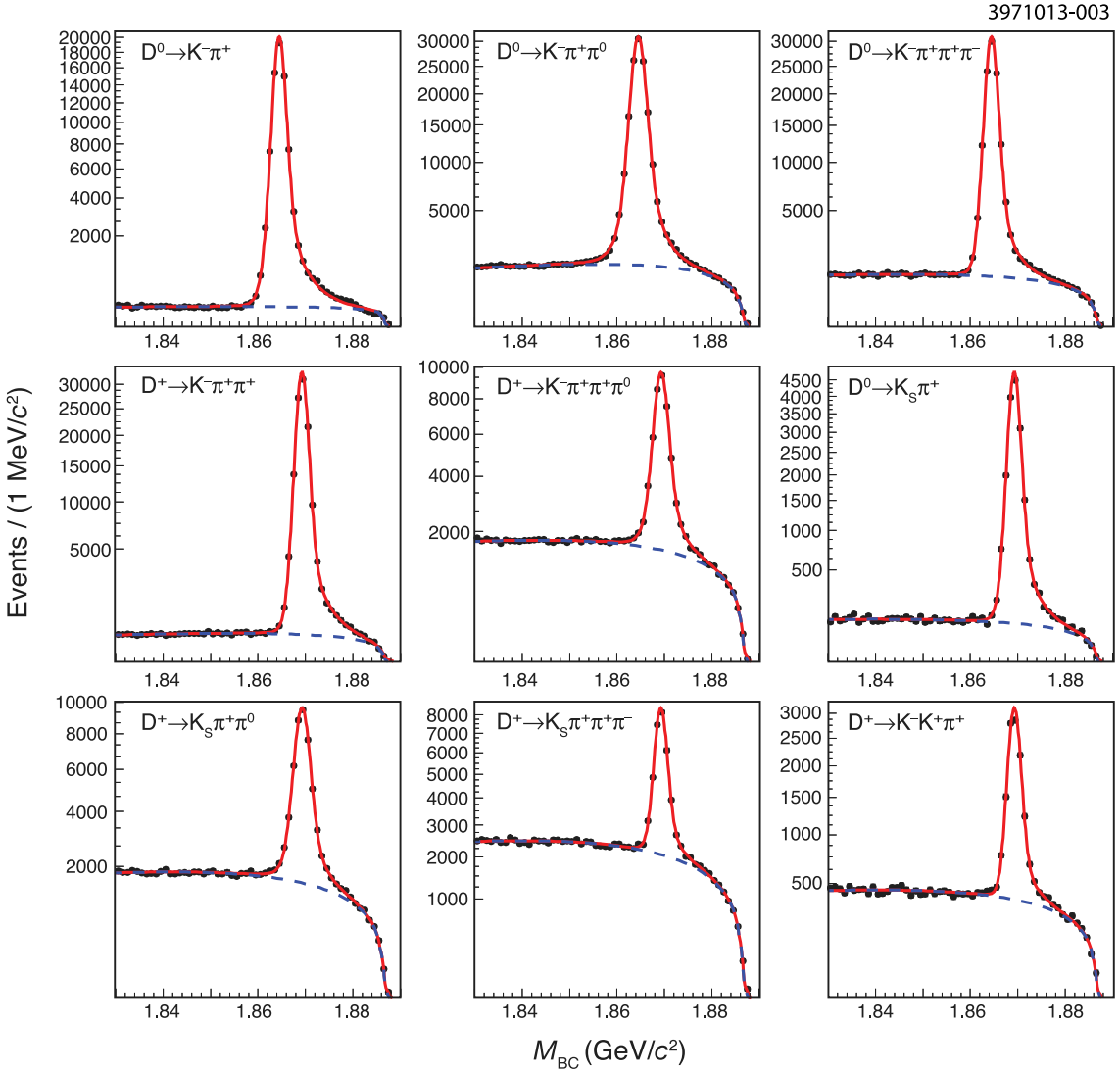


FIG. 1 (color online). Numbers of single tag event candidates, plotted on square-root scales, versus $M_{\rm BC}$ for each charged and neutral mode. In each plot, $D$ and $\bar{D}$ candidates are combined. Data are shown as points and the solid lines (red online) show the total fits and the dashed lines (blue online) are the background shapes. The high-mass tails on the signal are due to initial-state radiation.

in the signal regions that do contribute to these yields. In the branching fraction fit, we correct the ST and DT yields for two types of peaking backgrounds, which we call "internal" and "external." Internal or cross feed backgrounds come from decays to any one of our signal modes, $i$, that peak in the $M_{\rm BC}$ distributions of any other modes due to misreconstruction. This type of contribution to any signal mode is proportional to the branching fraction $\mathcal{B}_i$ for the misreconstructed decay mode and the appropriate $N_{D\bar{D}}$, both of which are determined in the fit. On the other hand, external backgrounds are from $D$ or $\bar{D}$ decays to modes that we do not measure in this analysis, but which appear in the peaks of signal modes due to misreconstruction. These contributions are proportional to the appropriate $N_{D\bar{D}}$ values that we obtain in the fit and the branching fractions for the modes that we obtain from the particle data group [18]. For both types of peaking background, we determine the relevant proportionality constants from Monte Carlo simulations. We iterate our fit to minimize $\chi^2$ and—at each iteration—we recalculate the internal and external peaking contributions using the $\mathcal{B}_i$ and $N_{D\bar{D}}$ values obtained in the previous iteration. These estimated peaking contributions produce yield adjustments of $\mathcal{O}(1\%)$.

## IV. SYSTEMATIC UNCERTAINTIES

We updated systematic uncertainties for the full 818 pb$^{-1}$ data sample, using methods described in Ref. [9]. The larger data sample has led to improvement of some systematic uncertainties measured in data. Some other systematic uncertainties were reduced by improvements in the techniques for their estimation. The resulting systematic uncertainties for ST yields for each $D^0$ and $D^+$ decay mode are given in Table II.

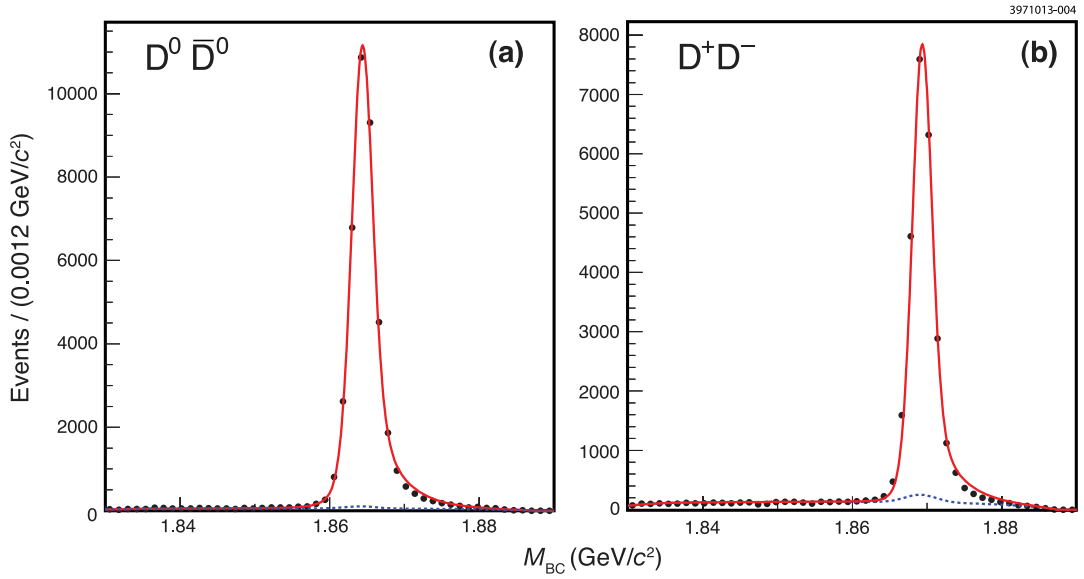


FIG. 2 (color online). Projections of double tag candidate masses on the $M_{\rm BC}(D)$ axis for (a) all $D^0\bar{D}^0$ modes and (b) all $D^+D^-$ modes. In each plot, the points are data, the lines are projections of the fit results; the dashed line (blue online) is the peaking background contribution, and the solid line (red online) is the sum of signal and background.

We assign a tracking systematic uncertainty of 0.3% per $\pi^\pm$ and 0.6% for $K^\pm$ candidate for all decay modes, including the $\pi^\pm$ produced in $K^0_S$ decay. These tracking uncertainties are correlated among all charged particles. There is a systematic uncertainty of 0.8% in the reconstruction efficiency $\epsilon(K^0_S)$ for neutral kaons that is correlated among all $K^0_S$ candidates.

In further studies following procedures described in Appendix B.5 of Ref. [9] we refined our understanding of small differences between the $\pi^0$ efficiencies in MC simulations and data. Based on these studies, the efficiencies for $D^0 \to K^-\pi^+\pi^0$, $D^+ \to K^-\pi^+\pi^+\pi^0$, $D^+ \to K^0_S\pi^+\pi^0$, and their charge conjugates in Table I include a correction factor of 0.939 with uncertainties of 1.3%, 1.5%, and 1.3%, respectively, reduced from 2% in Ref. [9].

Particle identification efficiencies are studied by reconstructing decays with unambiguous particle content, such as $D^0 \to K^0_S\pi^+\pi^-$ and $\phi \to K^+K^-$. The decay of $D^0 \to K^-\pi^+\pi^0$ is also used for the study, as the $K^-$ and $\pi^+$ can be distinguished kinematically. We require PID for all charged kaons and for all charged pions that are not the daughters of $K^0_S$ decay. We utilize the following techniques to account for the small differences observed between data and Monte Carlo simulations of PID. In each final state, we apply an efficiency correction factor 0.995 per PID-identified $\pi^\pm$ and 0.990 per

TABLE II. Contributions, in percent, to the systematic uncertainties for each ST efficiency-corrected yield, enumerated by decay mode. The first three modes are $D^0(\bar{D}^0)$ and the rest are $D^+(D^-)$ modes. $K$ and $\pi$ are shorthand for the appropriate charged kaons and pions in each decay mode. Each of the uncertainties in the last three rows are not correlated with any other uncertainties. The rest of the uncertainties are fully correlated among all modes within a row, but uncertainties in one row are not correlated with those in another. Efficiency uncertainties (denoted by $\epsilon$) are multiplicative and other (yield) uncertainties are additive.

| Source | $K\pi$ | $K\pi\pi^0$ | $K\pi\pi\pi$ | $K\pi\pi$ | $K\pi\pi\pi^0$ | $K^0_S\pi$ | $K^0_S\pi\pi^0$ | $K^0_S\pi\pi\pi$ | $KK\pi$ |
|---|---|---|---|---|---|---|---|---|---|
| $\epsilon$ (Tracking) | 0.90 | 0.90 | 1.50 | 1.20 | 1.20 | 0.90 | 0.90 | 1.50 | 1.50 |
| $\epsilon(K^0_S)$ | ··· | ··· | ··· | ··· | ··· | 0.80 | 0.80 | 0.80 | ··· |
| $\epsilon(\pi^0)$ | ··· | 1.30 | ··· | ··· | 1.50 | ··· | 1.30 | ··· | ··· |
| $\epsilon(\pi^\pm)$ PID | 0.25 | 0.25 | 0.75 | 0.50 | 0.50 | 0.25 | 0.25 | 0.75 | 0.25 |
| $\epsilon(K^\pm)$ PID | 0.30 | 0.30 | 0.30 | 0.30 | 0.30 | ··· | ··· | ··· | 0.60 |
| Lepton veto | 0.10 | ··· | ··· | ··· | ··· | ··· | ··· | ··· | ··· |
| FSR | 0.80 | 0.40 | 0.70 | 0.50 | 0.20 | 0.40 | 0.20 | 0.50 | 0.30 |
| Signal shape | 0.40 | 0.50 | 0.51 | 0.34 | 0.48 | 0.39 | 0.48 | 0.55 | 0.54 |
| Backg. shape | 0.38 | 1.10 | 0.76 | 0.40 | 3.05 | 0.77 | 1.53 | 1.22 | 0.82 |
| $\Delta E$ | 0.10 | 0.20 | 0.20 | 0.10 | 0.20 | 0.00 | 0.40 | 1.20 | 0.20 |
| Substructure | ··· | 0.58 | 1.30 | 0.53 | 0.94 | ··· | 0.42 | 0.62 | 2.60 |
| Mult. cand. | 0.00 | 0.70 | 0.00 | 0.00 | 0.20 | 0.20 | 0.00 | 0.00 | 0.00 |

TABLE III. Results of the fit to our data. The uncertainties quoted are statistical and systematic, respectively. Fractional uncertainties are also listed in separate columns.

| Parameter | Fitted value | Fractional error Stat.(%) | Syst.(%) |
|---|---|---|---|
| $N_{D^0\bar{D}^0}$ | $(2.951 \pm 0.014 \pm 0.035) \times 10^6$ | 0.5 | 1.2 |
| $\mathcal{B}(D^0 \to K^-\pi^+)$ | $(3.934 \pm 0.021 \pm 0.061)\%$ | 0.5 | 1.5 |
| $\mathcal{B}(D^0 \to K^-\pi^+\pi^0)$ | $(14.956 \pm 0.074 \pm 0.335)\%$ | 0.5 | 2.2 |
| $\mathcal{B}(D^0 \to K^-\pi^+\pi^+\pi^-)$ | $(8.287 \pm 0.043 \pm 0.200)\%$ | 0.5 | 2.4 |
| $N_{D^+D^-}$ | $(2.358 \pm 0.014 \pm 0.025) \times 10^6$ | 0.6 | 1.1 |
| $\mathcal{B}(D^+ \to K^-\pi^+\pi^+)$ | $(9.224 \pm 0.059 \pm 0.157)\%$ | 0.6 | 1.7 |
| $\mathcal{B}(D^+ \to K^-\pi^+\pi^+\pi^0)$ | $(6.142 \pm 0.045 \pm 0.154)\%$ | 0.7 | 2.5 |
| $\mathcal{B}(D^+ \to K^0_S\pi^+)$ | $(1.578 \pm 0.013 \pm 0.025)\%$ | 0.8 | 1.6 |
| $\mathcal{B}(D^+ \to K^0_S\pi^+\pi^0)$ | $(7.244 \pm 0.053 \pm 0.166)\%$ | 0.7 | 2.3 |
| $\mathcal{B}(D^+ \to K^0_S\pi^+\pi^+\pi^-)$ | $(3.051 \pm 0.027 \pm 0.082)\%$ | 0.9 | 2.7 |
| $\mathcal{B}(D^+ \to K^+K^-\pi^+)$ | $(0.981 \pm 0.010 \pm 0.032)\%$ | 1.0 | 3.2 |

$K^\pm$. We also assign systematic uncertainties of 0.25% to each PID-identified $\pi^\pm$ and 0.30% to each $K^\pm$, correlated among all charged PID-identified pions and kaons separately.

We assign a systematic uncertainty of 0.1% to $D^0 \to K^-\pi^+$ single tag yields to account for the lepton veto requirement. For FSR we allocate systematic uncertainties of 25% [19] of the correction for each mode, correlated across all modes. The systematic uncertainties, (0.4–1.5)%, for background shapes in single tag yields are estimated by using alternative ARGUS parameters.

Other sources of efficiency uncertainty include the following: the $\Delta E$ requirements (0.0–1.2)%, for which we examine $\Delta E$ sidebands; modeling of multiple candidates (0.0–0.7)%; and modeling of resonant substructure in multibody modes (0.4–2.6)%, which we assess by comparing simulated momentum spectra to those in data or changes in ST efficiency due to new measurements of resonant substructure.

The effects of quantum correlations between the $D^0$ and $\bar{D}^0$ states appear through $D^0 - \bar{D}^0$ mixing and doubly Cabibbo-suppressed decays [20]. We use the results reported in Refs. [21] and [22] to correct the $D^0$ and $\bar{D}^0$ yields for these effects. This reduces the systematic uncertainty previously attributed to quantum correlations from 0.8% to the range (0.1–0.4)%.

There is no significant deviation from 100% for the trigger efficiency in the MC simulation of the efficiency, so we no longer assign a systematic uncertainty to it.

The branching fraction fitter [12] takes these systematic uncertainties into account, along with ST and DT yields, efficiencies, peaking backgrounds, and their statistical uncertainties. We studied the validity of the fitter and our analysis technique [9] using a generic Monte Carlo sample, which had three times as many events as our data sample. The results of this study validated our entire analysis procedure, including the fitter.

## V. RESULTS AND CONCLUSIONS

The results of the branching fraction fit are given in Table III, where we have listed both statistical and systematical errors. The correlation matrix for the fitted parameters is listed in Table IV. We also compute the ratios of branching fractions with respect to the two "reference" modes as shown in Table V. The $\chi^2$ of the fit is 46.7 for 52

TABLE IV. The correlation matrix, including systematic uncertainties, for the fit results for $N_{D\bar{D}}$ and branching fractions. $K$ and $\pi$ are shorthand for the appropriate charged kaons and pions in each decay mode. The parameter order matches that in Table III.

| | $N_{D^0\bar{D}^0}$ | $K\pi$ | $K\pi\pi^0$ | $K\pi\pi\pi$ | $N_{D^+D^-}$ | $K\pi\pi$ | $K\pi\pi\pi^0$ | $K^0_S\pi$ | $K^0_S\pi\pi^0$ | $K^0_S\pi\pi\pi$ | $KK\pi$ |
|---|---|---|---|---|---|---|---|---|---|---|---|
| $N_{D^0\bar{D}^0}$ | 1.00 | −0.56 | −0.29 | −0.30 | 0.49 | −0.19 | −0.11 | −0.17 | −0.11 | −0.08 | −0.06 |
| $K\pi$ | | 1.00 | 0.52 | 0.75 | −0.23 | 0.69 | 0.45 | 0.51 | 0.36 | 0.51 | 0.41 |
| $K\pi\pi^0$ | | | 1.00 | 0.43 | −0.14 | 0.41 | 0.69 | 0.30 | 0.68 | 0.31 | 0.25 |
| $K\pi\pi\pi$ | | | | 1.00 | −0.13 | 0.65 | 0.42 | 0.47 | 0.33 | 0.51 | 0.37 |
| $N_{D^+D^-}$ | | | | | 1.00 | −0.50 | −0.21 | −0.51 | −0.28 | −0.27 | −0.24 |
| $K\pi\pi$ | | | | | | 1.00 | 0.50 | 0.70 | 0.45 | 0.63 | 0.50 |
| $K\pi\pi\pi^0$ | | | | | | | 1.00 | 0.38 | 0.65 | 0.37 | 0.29 |
| $K^0_S\pi$ | | | | | | | | 1.00 | 0.52 | 0.63 | 0.39 |
| $K^0_S\pi\pi^0$ | | | | | | | | | 1.00 | 0.43 | 0.25 |
| $K^0_S\pi\pi\pi$ | | | | | | | | | | 1.00 | 0.35 |
| $KK\pi$ | | | | | | | | | | | 1.00 |

TABLE V. Branching ratios from the fit to our data. The uncertainties quoted are statistical and systematic, respectively.

| Parameter | Fitted value | Fractional error Stat.(%) | Syst.(%) |
|---|---|---|---|
| $\mathcal{B}(D^0 \to K^-\pi^+\pi^0)/\mathcal{B}(K^-\pi^+)$ | $3.802 \pm 0.022 \pm 0.073$ | 0.6 | 1.9 |
| $\mathcal{B}(D^0 \to K^-\pi^+\pi^+\pi^-)/\mathcal{B}(K^-\pi^+)$ | $2.106 \pm 0.013 \pm 0.032$ | 0.6 | 1.5 |
| $\mathcal{B}(D^+ \to K^-\pi^+\pi^+\pi^0)/\mathcal{B}(K^-\pi^+\pi^+)$ | $0.666 \pm 0.006 \pm 0.014$ | 0.9 | 2.1 |
| $\mathcal{B}(D^+ \to K^0_S\pi^+)/\mathcal{B}(K^-\pi^+\pi^+)$ | $0.171 \pm 0.002 \pm 0.002$ | 1.0 | 0.9 |
| $\mathcal{B}(D^+ \to K^0_S\pi^+\pi^0)/\mathcal{B}(K^-\pi^+\pi^+)$ | $0.785 \pm 0.007 \pm 0.016$ | 0.9 | 2.1 |
| $\mathcal{B}(D^+ \to K^0_S\pi^+\pi^+\pi^-)/\mathcal{B}(K^-\pi^+\pi^+)$ | $0.331 \pm 0.004 \pm 0.006$ | 1.2 | 1.8 |
| $\mathcal{B}(D^+ \to K^+K^-\pi^+)/\mathcal{B}(K^-\pi^+\pi^+)$ | $0.106 \pm 0.002 \pm 0.003$ | 1.4 | 2.6 |

TABLE VI. *CP* asymmetry for each decay mode, in percent.

| Mode | *CP* asymmetry (%) |
|---|---|
| $D^0 \to K^-\pi^+$ | $0.3 \pm 0.3 \pm 0.6$ |
| $D^0 \to K^-\pi^+\pi^0$ | $0.1 \pm 0.3 \pm 0.4$ |
| $D^0 \to K^-\pi^+\pi^+\pi^-$ | $0.2 \pm 0.3 \pm 0.4$ |
| $D^+ \to K^-\pi^+\pi^+$ | $-0.3 \pm 0.2 \pm 0.4$ |
| $D^+ \to K^-\pi^+\pi^+\pi^0$ | $-0.3 \pm 0.6 \pm 0.4$ |
| $D^+ \to K^0_S\pi^+$ | $-1.1 \pm 0.6 \pm 0.2$ |
| $D^+ \to K^0_S\pi^+\pi^0$ | $-0.1 \pm 0.7 \pm 0.2$ |
| $D^+ \to K^0_S\pi^+\pi^+\pi^-$ | $0.0 \pm 1.2 \pm 0.3$ |
| $D^+ \to K^+K^-\pi^+$ | $-0.1 \pm 0.9 \pm 0.4$ |

degrees of freedom. These results supersede previous CLEO results [8,9], obtained utilizing subsets of the full 818 $\text{pb}^{-1}$ data sample, and are the most precise results reported to date [3].

The $e^+e^- \to D\bar{D}$ cross sections are obtained by dividing $N_{D^0\bar{D}^0}$ and $N_{D^+D^-}$ by the luminosity of our data set, $(818.1 \pm 8.2)$ $\text{pb}^{-1}$. The luminosity was determined using the procedure described in Appendix C of Ref. [9]. We find

$$\sigma(e^+e^- \to D^0\bar{D}^0) = (3.607 \pm 0.017 \pm 0.056)\ \text{nb} \quad (4)$$

$$\sigma(e^+e^- \to D^+D^-) = (2.882 \pm 0.018 \pm 0.042)\ \text{nb} \quad (5)$$

$$\sigma(e^+e^- \to D\bar{D}) = (6.489 \pm 0.024 \pm 0.092)\ \text{nb} \quad (6)$$

$$\sigma(e^+e^- \to D^+D^-)/\sigma(e^+e^- \to D^0\bar{D}^0) = 0.799 \pm 0.006 \pm 0.008, \quad (7)$$

where the uncertainties are statistical and systematic, respectively. The charged and neutral cross sections have a correlation coefficient of 0.69 stemming from the systematic uncertainties for $N_{D^0\bar{D}^0}$, $N_{D^+D^-}$, and the luminosity measurement. For this reason, the uncertainty on $\sigma(e^+e^- \to D\bar{D})$ is larger than the quadratic sum of the charged and neutral cross section uncertainties.

For each decay mode $f$ and its charge conjugate $\bar{f}$, we obtain the *CP* asymmetry,

$$A_{CP}(f) \equiv \frac{n(f) - n(\bar{f})}{n(f) + n(\bar{f})}, \quad (8)$$

from the single tag yields, $n(f)$ and $n(\bar{f})$, obtained after subtraction of backgrounds and correction for efficiencies [9]. Table VI gives the values of $A_{CP}(f)$ obtained from the full 818 $\text{pb}^{-1}$ data sample. No mode shows evidence of *CP* violation at the level of the uncertainties, which are of order 1% for all modes. Standard model estimates of *CP* violation are at most a few tenths of a percent [23] and we are not sensitive to asymmetries at this level.

In summary, we report measurements of three $D^0$ and six $D^+$ branching fractions and the production cross sections $\sigma(D^0\bar{D}^0)$, $\sigma(D^+D^-)$, and $\sigma(D\bar{D})$ using a sample of 818 $\text{pb}^{-1}$ of $e^+e^- \to D\bar{D}$ data obtained at $E_{\text{cm}} = 3774 \pm 1$ MeV.

## ACKNOWLEDGMENTS

We gratefully acknowledge the effort of the CESR staff in providing us with excellent luminosity and running conditions. This work was supported by the National Science Foundation, the U. S. Department of Energy, the Natural Sciences and Engineering Research Council of Canada, and the U. K Science and Technology Facilities Council. X. Shi thanks the High Energy Group National Taiwan University National Science Council where part of this work was completed.

[1] N. Cabibbo, Phys. Rev. Lett. **10**, 531 (1963).
[2] M. Kobayashi and T. Maskawa, Prog. Theor. Phys. **49**, 652 (1973).
[3] J. Beringer *et al.* (Particle Data Group), Phys. Rev. D **86**, 010001 (2012).
[4] Y. Kubota *et al.* (CLEO Collaboration), Nucl. Instrum. Methods Phys. Res., Sect. A **320**, 66 (1992).
[5] D. Peterson *et al.*, Nucl. Instrum. Methods Phys. Res., Sect. A **478**, 142 (2002).
[6] M. Artuso *et al.*, Nucl. Instrum. Methods Phys. Res., Sect. A **554**, 147 (2005).
[7] CLEO-c/CESR-c Taskforces & CLEO-c Collaboration, Cornell LEPP Report No. CLNS 01/1742, 2001 (unpublished).
[8] Q. He *et al.* (CLEO Collaboration), Phys. Rev. Lett. **95**, 121801 (2005).
[9] S. Dobbs *et al.* (CLEO Collaboration), Phys. Rev. D **76**, 112001 (2007).
[10] R. M. Baltrusaitis *et al.* (MARK-III Collaboration), Phys. Rev. Lett. **56**, 2140 (1986).
[11] J. Adler *et al.* (MARK-III Collaboration), Phys. Rev. Lett. **60**, 89 (1988).
[12] W. M. Sun, Nucl. Instrum. Methods Phys. Res., Sect. A **556**, 325 (2006).
[13] R. Brun, F. Carminati, and S. Giani, GEANT 3.21, CERN Program Library Long Writeup Report No. W5013 (unpublished).
[14] D. J. Lange, Nucl. Instrum. Methods Phys. Res., Sect. A **462**, 152 (2001).
[15] E. Barberio and Z. Was, Comput. Phys. Commun. **79**, 291 (1994), version 2.15 with interference enabled.
[16] H. Albrecht *et al.* (ARGUS Collaboration), Phys. Lett. B **241**, 278 (1990).
[17] W. Verkerke and D. Kirkby, eConf No. C0303241 (2003) [for documentation and source code, see http://roofit.sourceforge.net/].
[18] K. Nakamura (Particle Data Group), J. Phys. G **37**, 075021 (2010).
[19] D. Asner *et al.* (Heavy Flavor Averaging Group), arXiv:1010.1589v2.
[20] D. M. Asner and W. M. Sun, Phys. Rev. D **73**, 034024 (2006); D. M. Asner and W. M. Sun, Phys. Rev. D **77**, 019901(E) (2008).
[21] A. Schwartz *et al.* (Heavy Flavor Averaging Group), http://www.slac.stanford.edu/xorg/hfag/.
[22] N. Lowrey *et al.* (CLEO Collaboration), Phys. Rev. D **80**, 031105 (2009).
[23] S. Bianco, F. L. Fabbri, D. Benson, and I. Bigi, Nuovo Cimento Soc. Ital. Fis. **26N7**, 1 (2003).